



Study on the correlation between microstructural evolution and hydrogen storage properties in hyper-eutectic Mg-xNi ($x = 15, 20, 25$) alloys

So Jin Jung ^{a,b}, Seok Su Sohn ^b, Da Hye Lee ^{a,b}, Won-Seok Ko ^c, Tae Jun Ha ^{a, ID},
Ryun-Ho Kwak ^{a,b}, Byeong-Chan Suh ^{d, **}, Young Min Kim ^{d, ***}, Hyung-Ki Park ^{a, * ID}

^a Functional Materials and Components Group, Korea Institute of Industrial Technology, Gangneung, 25440, Republic of Korea

^b Department of Materials Science and Engineering, Korea University, Seoul, 02841, Republic of Korea

^c Department of Materials Science and Engineering, Inha University, Incheon, 22212, Republic of Korea

^d Lightweight Materials Research Division, Korea Institute of Materials Science, Changwon, 51508, Republic of Korea



ARTICLE INFO

Handling editor: L Murr

Keywords:

Mg–Ni alloy
Hydrogen storage alloy
Plateau pressure
Hydrogen storage property
Hyper-eutectic alloy

ABSTRACT

This study investigated the effect of Ni content on the microstructure and hydrogen storage properties of hyper-eutectic Mg–Ni hydrogen storage alloys. Mg-xNi ($x = 15, 20, 25$ (at%)) alloys were prepared using vacuum induction melting. These alloys consisted of a primary Mg₂Ni phase and an Mg–Mg₂Ni lamellar structure, with the proportion of the primary Mg₂Ni phase increasing as the Ni content rose. The hydrogen absorption and desorption behaviors of the alloys were analyzed at 325 °C. The maximum hydrogen storage capacity of the Mg–15Ni alloy was 5.29 wt%. As the Ni content increased, the phase percentage of the Mg₂Ni phase increased, leading to a reduction in the maximum hydrogen storage capacities of the Mg–20Ni and Mg–25Ni alloys to 5.01 and 4.67 wt%, respectively. Although the maximum hydrogen storage capacity varied with Ni content, both the first plateau pressure (Mg → MgH₂) and the second plateau pressure (Mg₂Ni → Mg₂NiH₄) during hydrogen absorption remained unchanged and consistent across all three alloys. To understand why the plateau pressure remained constant despite variations in alloy composition, the equilibrium compositions of the Mg and Mg₂Ni phases in the alloys were calculated through thermodynamic calculations. In addition, the compositions of the Mg and Mg₂Ni phases within the lamellar structure were analyzed using transmission electron microscope. These analyses confirmed that, despite variations in Ni content across the alloys, the chemical composition of the individual Mg and Mg₂Ni phases remained unchanged. The Mg phase exhibited a 100% Mg composition, while the Mg₂Ni phase showed an atomic ratio of Mg to Ni of 2:1, closely matching the theoretical stoichiometric ratio. In hydrogen storage alloys, plateau pressures are influenced by the composition of each phase rather than the overall composition of the alloy. Consequently, even with changes in Ni content in the hyper-eutectic Mg–Ni alloys, the plateau pressures remained unchanged. When Ni is added to Mg hydrogen storage alloys, the hydrogen reaction kinetics are improved. However, this study confirmed that, despite the increase in Ni content, the plateau pressures remained unchanged, while the maximum hydrogen storage capacities decreased. Therefore, it is essential to derive an optimal Mg–Ni alloy composition that balances both reaction kinetics and hydrogen storage capacity.

1. Introduction

Hydrogen storage alloys are materials designed to store hydrogen efficiently through absorption, resulting in a phase transformation to a metal hydride phase [1]. These alloys are notable for their high volumetric storage density and the ability to store hydrogen at relatively low

pressures, making them suitable for the safe storage of large hydrogen quantities [2,3]. Hydrogen storage alloys consist of A elements that react with hydrogen to form a metal hydride phase and B elements that do not react with hydrogen. The properties related to hydrogen storage can be fine-tuned by modifying the composition and the ratio of elements A and B [4,5]. The classification of these alloys is based on their composition,

* Corresponding author.

** Corresponding author.

*** Corresponding author.

E-mail addresses: bcuh@kims.re.kr (B.-C. Suh), ymkim@kims.re.kr (Y.M. Kim), mse03@kitech.re.kr (H.-K. Park).

with TiFe, TiMn₂, LaNi₅, and Mg-based alloys serving as notable compositions.

Hydrogen storage alloys exhibit similar volumetric storage densities, ranging between 100 and 120 kg-H₂/m³. However, their gravimetric storage density varies according to the material's density [6]. Magnesium (Mg), known for its low density and lightness, offers a high gravimetric storage density of 7.6 wt%, making it superior to other hydrogen storage alloys in this aspect [7]. This advantage positions Mg as a promising candidate for both mobile and stationary hydrogen storage applications. Nonetheless, Mg-based storage alloys face challenges, particularly the necessity for high temperatures (>300 °C) to release hydrogen because of their high enthalpy (~75 kJ/mol) of the Mg + H₂ ↔ MgH₂ reaction [8]. Furthermore, the reaction rate is slow, leading to extended durations required for hydrogen absorption and release. Consequently, extensive research efforts are directed toward lowering the hydrogen desorption temperature and accelerating the reaction rate in Mg-based storage alloys.

Research has highlighted the potential for post-processing techniques to enhance the hydrogen reaction rate in Mg-based hydrogen storage alloys. In particular, it has been found that the application of plastic deformations to hydrogen storage alloys can lead to an increased rate of hydrogen diffusion, a phenomenon attributed to the formation of defects [9,10]. Consequently, various studies have explored the application of plastic deformation methods, such as high-energy ball milling and severe plastic deformation, to these alloys [11–13]. These methods have been shown to improve the kinetics of hydrogen absorption and desorption. However, despite the benefits of hydrogen kinetics, the implementation of plastic deformation techniques presents significant challenges, as the process requires substantial time and energy.

Furthermore, the hydrogen storage performance of Mg-based storage alloy can be enhanced by alloying with transition metals [14]. Alloying Mg with iron (Fe) results in the formation of an Mg₂Fe phase, which exhibits a hydrogen storage capacity of 5.47 wt%. This addition can significantly improve the kinetics of hydrogen absorption and desorption [15]. Nonetheless, the release of hydrogen from this alloy still requires high temperatures because of the high dehydrogenation enthalpy of the Mg₂FeH₆ phase, estimated at approximately 80.0 kJ/mol [16]. Moreover, the challenge of alloying Mg with Fe stems from the large positive mixing enthalpy between these two elements. This thermodynamic characteristic prevents the fabrication of Mg–Fe hydrogen storage alloys using conventional casting methods. These alloys can be synthesized using the mechanical alloying method; however, this approach is limited by challenges related to process efficiency and scalability [17, 18].

Contrastingly, Mg–Ni binary alloys benefit from a more straightforward fabrication process via conventional casting methods, with Nickel (Ni) addition to Mg enhancing the hydrogen reaction kinetics [19,20]. Furthermore, the hydride-forming enthalpy of the Mg₂Ni phase in Mg–Ni hydrogen storage alloys is relatively low, at 64.4 kJ/mol, which facilitates a reduction in hydrogen desorption temperature [21]. According to the Mg–Ni binary phase diagram (Fig. 1), the composition of the eutectic reaction is identified as Mg-11.3Ni (in at%). For hypo-eutectic compositions, where the Ni content is less than 11.3 at%, the alloy structure is characterized by the primary Mg phase and the Mg–Mg₂Ni lamellar structure [22]. In contrast, hyper-eutectic compositions, which have a higher Ni content, predominantly feature the primary Mg₂Ni phase alongside the Mg–Mg₂Ni lamellar structure [23, 24]. Research indicates that Mg–Ni alloys exhibit the improved hydrogen reaction kinetics across all compositions. In particular, hyper-eutectic alloys demonstrate superior hydrogen desorption kinetics and enhanced stabilities for repetitive hydrogen storage [25,26].

Despite the recognized benefits of Ni addition to Mg in enhancing hydrogen storage properties, there has been no reported investigation into how these properties vary Ni content in hyper-eutectic Mg–Ni hydrogen storage alloys. Therefore, in this study, we investigated the effects of Ni content on the hydrogen storage properties of hyper-

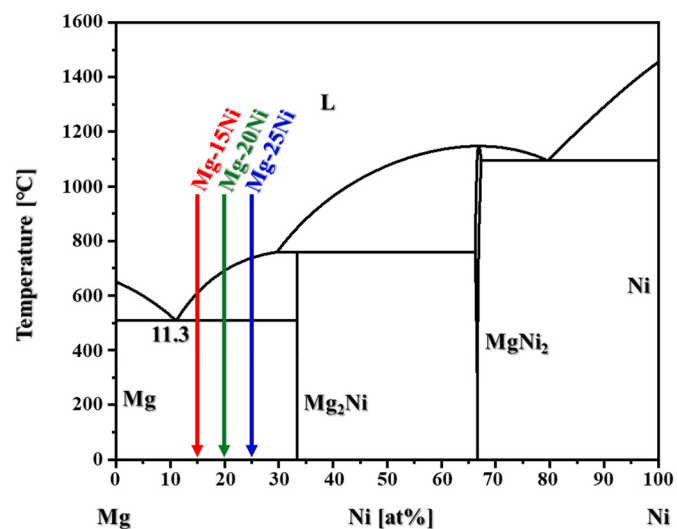


Fig. 1. Binary phase diagram of Mg–Ni alloy calculated Thermo-Calc software. Red, green, and blue lines indicate the compositions of Mg–15Ni, Mg–20Ni, and Mg–25Ni, respectively.

eutectic Mg–Ni alloys. In particular, Mg–xNi ($x = 15, 20, 25$ (at%)) alloys were examined to observe how their microstructure differs according to composition and to understand the formation of microstructures through thermodynamic calculations. Furthermore, the hydrogen storage properties of these alloys were assessed, analyzing the relationship between changes in hydrogen storage properties and their microstructures.

2. Experimental procedures

2.1. Sample preparation

Mg–xNi ($x = 15, 20, 25$ (at%)) alloys were produced through vacuum induction melting within a graphite crucible. The binary phase diagram for the Mg–Ni system, as indicated in Fig. 1, shows that the compositions of Mg–15Ni, Mg–20Ni, and Mg–25Ni fall within the hyper-eutectic range. For the melting process, high-purity materials were utilized: 99.99% Mg ingots and 99.99% Ni lumps. The manufacturing process began with loading the pure Mg ingot into the graphite crucible, which was then heated to 850 °C under a protective atmosphere composed of gas (10% SF₆ and 90% CO₂). Following this, Ni lumps (length × width × height = 30 × 30 × 3 mm) were introduced into the molten Mg, and a stainless steel rod facilitated stirring to ensure a homogenous molten mixture. Subsequently, the molten metal was cooled and then cast into bars, each having a diameter of 55 mm.

2.2. Microstructure analysis method

The phase analysis of Mg–15Ni, Mg–20Ni, and Mg–25Ni alloys was conducted utilizing an X-ray diffractometer (XRD) from PANalytical, specifically the Empyrean model. To observe the microstructures of these alloys, a field emission-scanning electron microscope (FE-SEM) was used, specifically the QUANTA FEG 250 model made by FEI, which was equipped with an energy dispersive spectrometer (EDS) for elemental analysis. Further detailed examination of the lamellar structures within the alloys was performed using a transmission electron microscope (TEM) of the JEOL, JEM-ARM 200F. For TEM analysis, sample preparation was carried out with focused ion beam (FIB) equipment, namely, the ZEISS Crossbeam350, which allows for precise sectioning of the material for detailed examination. To calculate the equilibrium phase percentages and compositions within these alloys, the Thermo-Calc software was employed, utilizing the Mg-based alloy

databases (TCMG7). This combination of advanced analytical techniques and computational tools provided comprehensive insights into the microstructural and phase characteristics of the Mg–Ni alloys.

2.3. Hydrogen storage property analysis method

The hydrogen storage properties of the alloys were assessed using Sieverts-type pressure-composition-temperature (PCT) measurement equipment, specifically the MICROTRAC MRB BELSORP HP model. To prepare for PCT analysis, the alloys were machined into chip form, and 0.5 g of these chip samples were loaded into the PCT sample chamber. The chamber was initially evacuated for 1 h to remove any existing gases. Subsequently, it was pressurized with 60 bar of hydrogen gas. To facilitate the first hydrogenation process, the sample chamber was heated to 300 °C and maintained at this temperature for 24 h. The hydrogen within the samples was removed by evacuating the chamber while maintaining a temperature of 350 °C. After that, hydrogen absorption and desorption behaviors were meticulously analyzed at a temperature of 325 °C.

3. Results and discussion

3.1. Microstructure formation of hyper-eutectic Mg–Ni alloys

Fig. 2 presents the XRD patterns for the Mg–xNi ($x = 15, 20, 25$) alloys, illustrating the dual-phase microstructure comprising both Mg and Mg₂Ni phases. With increasing Ni content, there noticeable changes in the peak intensities were observed: the peaks corresponding to the Mg phase diminished, while those associated with the Mg₂Ni phase became more pronounced. To accurately determine the phase percentages relative to the Ni content, the XRD patterns were analyzed using the Rietveld refinement method. The phase percentages of the Mg and Mg₂Ni phases in the three alloys are presented in **Table 1**. In particular, the percentages of the Mg phase in the Mg–15Ni, Mg–20Ni, and Mg–25Ni alloys were found to be 48.3, 32.6, and 21.4 wt%, respectively. Concurrently, the Mg₂Ni phase percentages in these alloys were quantified as 51.7, 67.4, and 78.6 wt% for Mg–15Ni, Mg–20Ni, and Mg–25Ni, respectively. This data highlights a clear trend of increasing Mg₂Ni phase percentage with higher Ni content, emphasizing the significant impact of Ni content on the phase formation behavior in hyper-eutectic Mg–Ni alloys.

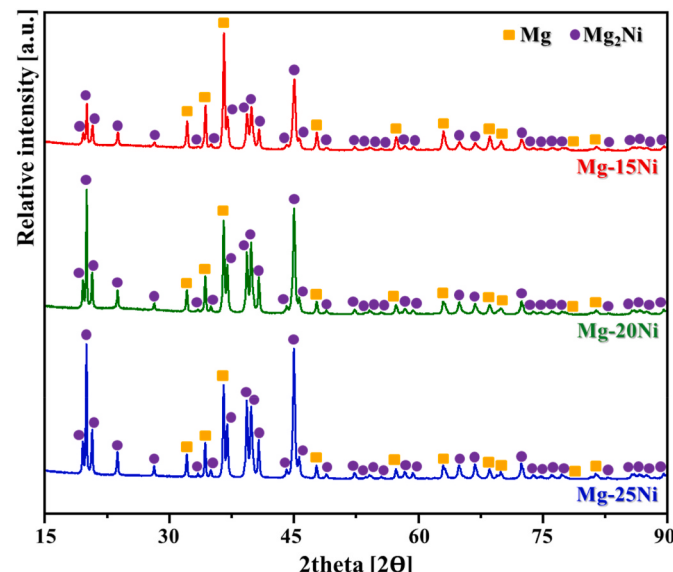


Fig. 2. XRD patterns of the Mg–15Ni, Mg–20Ni, and Mg–25Ni hydrogen storage alloys.

Table 1

Phase percentages of the Mg and Mg₂Ni phases in Mg–xNi alloys ($x = 15, 20, 25$) derived from the Rietveld refinement method and the thermodynamic calculations.

	Alloy	Phase percentage [wt%]	
		Mg	Mg ₂ Ni
XRD	Mg–15Ni	48.5	51.7
	Mg–20Ni	32.6	67.4
	Mg–25Ni	21.4	78.6
Thermodynamic calculation	Mg–15Ni	45.4	54.6
	Mg–20Ni	31.2	68.8
	Mg–25Ni	18.5	81.5

The lattice parameters for both the Mg and Mg₂Ni phases in the three alloys were accurately determined using the Rietveld refinement method, with the results detailed in **Table 2**. For the Mg phase, the lattice parameters a and b were both measured at 3.21 Å, while the c parameter was 5.21 Å. In contrast, the Mg₂Ni phase exhibited larger lattice parameters, with a and b both at 5.21 Å and c significantly larger at 13.27 Å. The analysis reveals that the lattice parameters of the Mg₂Ni phase are notably larger than those of the Mg phase. Interestingly, despite variations in Ni content across the Mg–15Ni, Mg–20Ni, and Mg–25Ni alloys, the lattice parameters for both the Mg and Mg₂Ni phases remained constant in all three alloys. This consistency suggests that changes in Ni content did not affect the lattice parameter of the individual phases within the hyper-eutectic Mg–Ni alloys.

Fig. 3 presents the microstructures of the Mg–xNi ($x = 15, 20, 25$) alloys, as observed through FE-SEM. The compositions of the phases marked the yellow dotted areas in **Fig. 3(a)**, **(b)**, and **(c)** were analyzed via EDS, yielding compositions of 66.46 Mg–33.54Ni, 66.32 Mg–33.68Ni, and 66.54 Mg–33.46Ni (in at%), respectively, which are consistent with the Mg₂Ni phase. The alloys consisted of the primary Mg₂Ni phase and Mg–Mg₂Ni lamellar structure, and these microstructure formation behaviors are consistent with previous studies on the microstructure of hyper-eutectic Mg–Ni alloys [27]. With increasing Ni content, the phase proportion of the primary Mg₂Ni phase increased, while that of the Mg–Mg₂Ni lamellar structure decreased. According to **Fig. 1**, the solidification sequence of hyper-eutectic Mg–Ni alloys follows L → L + Mg₂Ni → Mg + Mg₂Ni, indicating that the primary Mg₂Ni phase forms initially, followed by the formation of the Mg–Mg₂Ni lamellar structure. The microstructures shown in **Fig. 3** confirmed the phase formation sequence predicted by the phase diagram.

3.2. Hydrogen storage properties of hyper-eutectic Mg–Ni alloys

Fig. 4 displays the PCT curves of the Mg–xNi ($x = 15, 20, 25$) alloys, illustrating the hydrogen absorption and desorption behaviors. The alloys demonstrated maximum hydrogen storage capacities of 5.29 wt% for Mg–15Ni, 5.01 wt% for Mg–20Ni, and 4.67 wt% for Mg–25Ni. Notably, the theoretical hydrogen storage capacities for the Mg and Mg₂Ni phases are 7.6 wt% and 3.6 wt%, respectively [28]. The decrease in maximum hydrogen storage capacities with increasing Ni content in the Mg–Ni alloys was attributed to the reduction in the phase percentage of the Mg phase, which has a higher hydrogen storage capacity.

Table 2

Lattice parameters of the Mg and Mg₂Ni phases in the Mg–xNi ($x = 15, 20, 25$) alloys analyzed by the Rietveld refinement method.

Alloy	Phases	Lattice parameter [Å]
Mg–15Ni	Mg (hexagonal)	$a, b: 3.21/c: 5.21$
	Mg ₂ Ni (hexagonal)	$a, b: 5.21/c: 13.27$
Mg–20Ni	Mg (hexagonal)	$a, b: 3.21/c: 5.21$
	Mg ₂ Ni (hexagonal)	$a, b: 5.21/c: 13.27$
Mg–25Ni	Mg (hexagonal)	$a, b: 3.21/c: 5.21$
	Mg ₂ Ni (hexagonal)	$a, b: 5.21/c: 13.27$

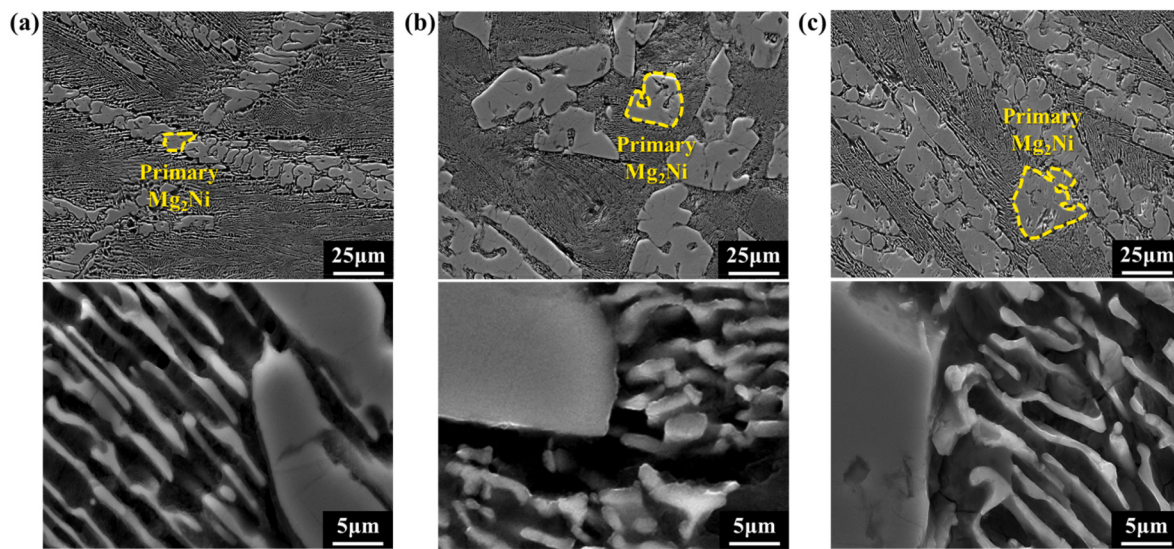


Fig. 3. Microstructures of (a) Mg-15Ni, (b) Mg-20Ni, and (c) Mg-25Ni alloys with enlarged microstructures presented below.

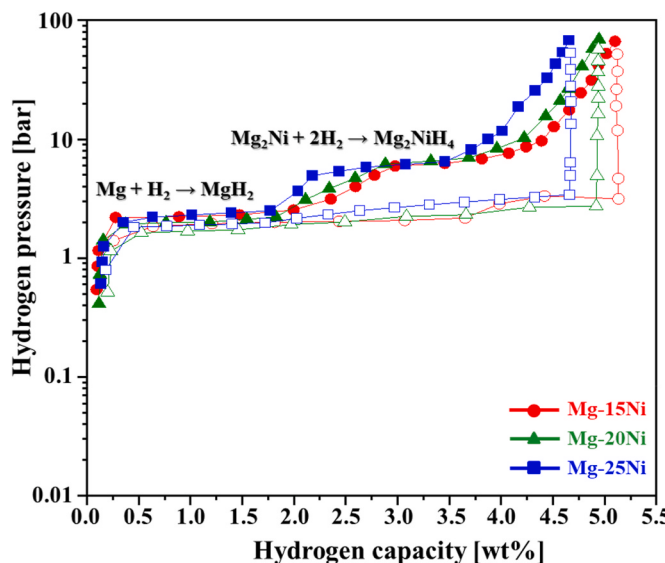


Fig. 4. PCT results analyzed at 325 °C for the Mg-xNi ($x = 15, 20, 25$) alloys.

During hydrogen absorption, the Mg–Ni alloys exhibited two distinct plateau pressures, attributable to the presence of the Mg and Mg_2Ni phases, each with different hydride-forming enthalpies. The first plateau pressure corresponds to the phase transformation of the Mg phase into the MgH_2 hydride phase, while the second plateau pressure results from the transformation of the Mg_2Ni phase into the Mg_2NiH_4 hydride phase. Notably, despite variations in Ni content across the three alloys, both the first and second plateau pressures remained constant.

Hydrogen storage alloy consists of two types of elements: element A, which reacts with hydrogen to form a hydride phase, and element B, which does not react with hydrogen. The plateau pressure represents the pressure at which hydrogen is stored in the hydrogen storage alloys and is a critical characteristic of these alloys. Consequently, extensive studies have been undertaken to manipulate the plateau pressure, primarily through adjusting the composition and ratio of elements A and B [3,4, 29–31]. Typically, an increase in the content of element B leads to a rise in plateau pressure, attributed to the reduced bonding energy between the hydrogen storage alloy and hydrogen. However, the hydrogen absorption and desorption behavior of the three alloys illustrated in Fig. 4

showed that the plateau pressure remained unaffected by changes in the Ni content.

3.3. Phase formation behavior predicted by thermodynamic calculations

To understand the microstructure changes as a function of Ni content, the phase formation behaviors of the Mg-xNi ($x = 15, 20, 25$) alloys were scrutinized via thermodynamic calculations. Fig. 5 illustrates the equilibrium phase formation behaviors of the three alloys as a function of temperature. In each alloy, the primary Mg_2Ni phase precipitated first from the liquid phase, followed by the formation of a dual-phase structure consisting of Mg and Mg_2Ni . The equilibrium phase percentages of the Mg and Mg_2Ni phase in the alloys are shown in Table 1. With increasing Ni content, the phase percentage of the Mg_2Ni phase increased, while that of the Mg correspondingly decreased. The theoretical percentages for the Mg phase in the Mg-15Ni, Mg-20Ni, and Mg-25Ni samples were found to be 45.4, 31.2, and 28.5 wt%, respectively, which closely align with the phase percentages derived from the XRD analyses.

Despite variations in Ni content, which led to changes in the percentages of the Mg and Mg_2Ni phases, both the first ($\text{Mg} \rightarrow \text{MgH}_2$) and second ($\text{Mg}_2\text{Ni} \rightarrow \text{Mg}_2\text{NiH}_4$) absorption plateau pressures remained constant, as depicted in Fig. 4. The plateau pressure is more influenced by the individual compositions of the Mg and Mg_2Ni phases than by the overall composition of the alloy. Therefore, even with changes in the alloy's Ni content, the plateau pressures could remain unchanged if the compositions of the Mg and Mg_2Ni phases remain constant. Consequently, the theoretical compositions of these two phases in the alloys were calculated and are presented in Fig. 6.

Fig. 6(a) illustrates the equilibrium Mg and Ni contents in the Mg phase of the alloys. Remarkably, for all three alloys, the Mg content was calculated at 100 at%, while the Ni content was 0 at%, indicating that the Mg phase in all three alloys is pure Mg without any Ni incorporation. The equilibrium Mg and Ni contents within the Mg_2Ni phases are detailed in Fig. 6(b). Consistently, across the three alloys, the Mg to Ni ratio in the Mg_2Ni phase was maintained at 2:1, perfectly matching the stoichiometry ratio of the Mg_2Ni phase. These thermodynamic calculation results suggest that, despite variations in the Ni content among the three alloys, the compositions of the Mg and Mg_2Ni phases remain unchanged.

The SEM-EDS analysis, as depicted in Fig. 3, confirmed that the primary Mg_2Ni phase in all three alloy maintained a Mg_2Ni composition. However, the interlamellar spacing in the Mg– Mg_2Ni lamellar structure

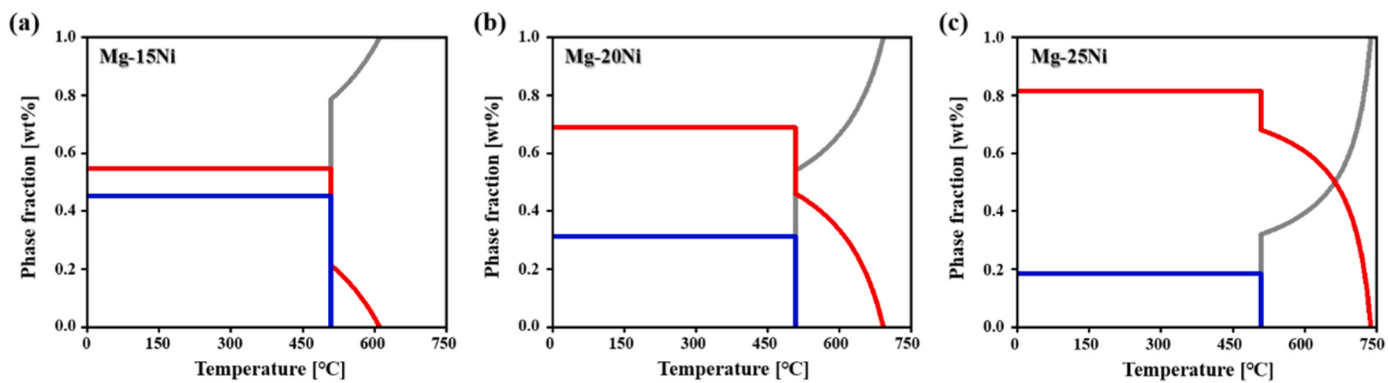


Fig. 5. Equilibrium phase percentages with respect to the temperature for the (a) Mg-15Ni, (b) Mg-20Ni, and (c) Mg-25Ni alloys.

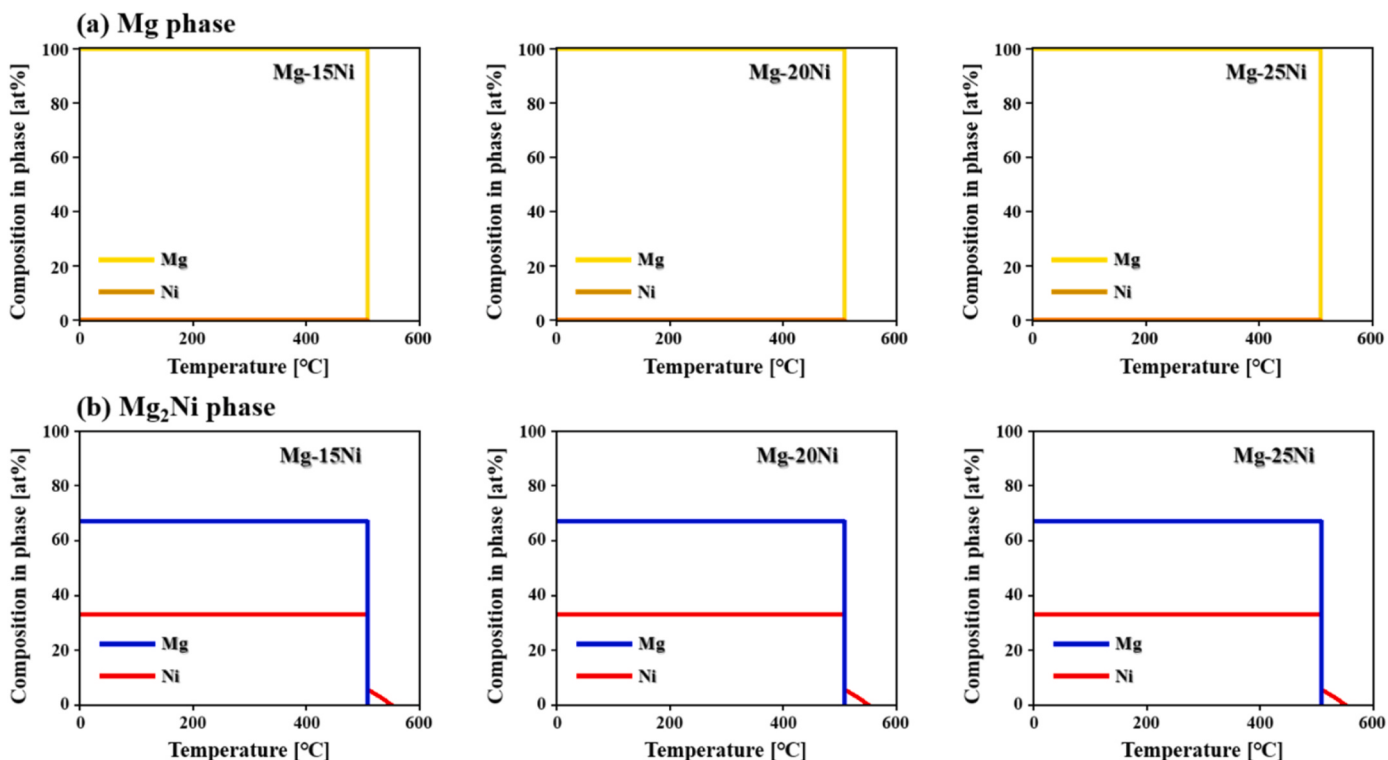


Fig. 6. Equilibrium Mg and Ni contents of the (a) Mg and (b) Mg₂Ni phases in the Mg-xNi ($x = 15, 20, 25$) alloys.

is too fine, making it difficult to accurately analyze the composition by SEM-EDS. To examine the composition of the Mg and Mg₂Ni phase in the lamellar structure, TEM analysis was conducted.

3.4. TEM analysis of Mg–Mg₂Ni lamellar structure in hyper-eutectic Mg–Ni alloys

Fig. 7 illustrates the microstructure of the Mg–Mg₂Ni lamellar structure in the Mg–15Ni alloy observed by TEM. TEM analyses were performed on the lamellar structures of the Mg–20Ni and Mg–25Ni alloys as well, revealing identical results to those of the Mg–15Ni alloy; thus, only the findings for the Mg–15Ni alloy were presented. The lamellar structure is characterized by light and dark phases. TEM-EDS analysis was conducted to determine the compositions of each phase within the Mg–15Ni, Mg–20Ni, and Mg–25Ni alloys, with the results detailed in Table 3. In the Mg–15Ni alloy, the composition of the bright phase was 100% Mg, while that of the dark phase was 65.47 Mg–34.53Ni (in at%), corresponding to the Mg₂Ni phase. Diffraction patterns for each phase were also analyzed and are displayed alongside Fig. 7, further

confirming that the bright and dark phases corresponded to the Mg and Mg₂Ni phases, respectively.

In the Mg–15Ni, Mg–20Ni, and Mg–25Ni alloys, the composition of the Mg phase was consistently 100% Mg, and that of the Mg₂Ni phases closely matched their theoretical composition. Such a result aligns with the thermodynamic calculation results (Fig. 6), indicating that despite variations in Ni content, the compositions of the Mg and Mg₂Ni phases remained unchanged. The XRD analysis results (Table 2) further supported this, showing identical lattice parameters for the Mg and Mg₂Ni phases across the three alloys. Given that the atomic sizes of Mg and Ni are 1.50 and 1.35 Å, respectively [32], any change in the compositions of the Mg and Mg₂Ni phases would typically result in a change in the lattice constants because of the differences in atomic sizes. However, the consistent lattice parameters observed across the samples suggest that the composition of each phase remained constant, thereby keeping the lattice constants unchanged. This consistency across different analytical methods reinforces the conclusion that the compositions of the two phases remained constant across the varying Ni contents in these alloys.

In hyper-eutectic Mg–Ni hydrogen storage alloys, as the Ni content

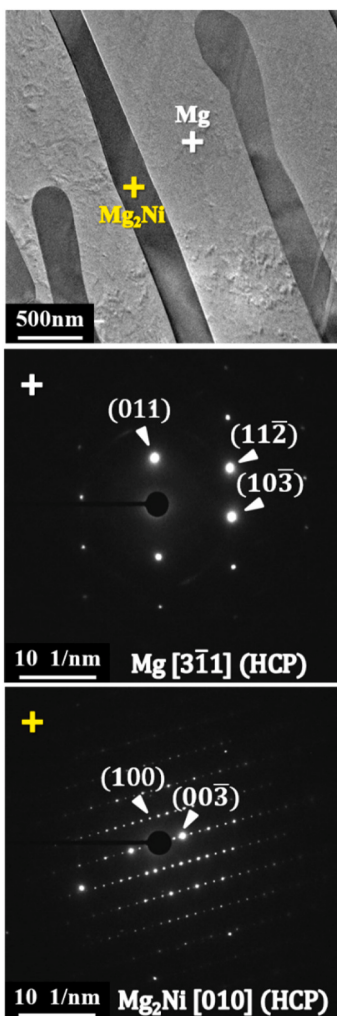


Fig. 7. TEM analysis results of the Mg–Mg₂Ni lamellar structure in the Mg–15Ni hydrogen storage alloy.

Table 3

The compositions of the Mg and Mg₂Ni phases in the lamellar structure of the Mg–xNi ($x = 15, 20, 25$) alloys analyzed by TEM- EDS.

Alloy	Composition [at%]			
	Mg phase		Mg ₂ Ni phase	
	Mg	Ni	Mg	Ni
Mg–15Ni	100	0	65.47	34.53
Mg–20Ni	100	0	65.40	34.60
Mg–25Ni	100	0	64.73	35.27

increased, the percentage of the Mg₂Ni phase increased, resulting in a reduction in the maximum hydrogen storage capacity. However, the plateau pressure remained unaffected by changes in Ni content, showing consistent values across all three alloys. The unchanged composition of the Mg and Mg₂Ni phases, despite variations in Ni content, suggests that the binding energy between the phases in the alloys and hydrogen remained constant. Therefore, the plateau pressure remained unchanged, despite variations in the Ni content of the alloys.

4. Conclusions

The hyper-eutectic Mg–xNi ($x = 15, 20, 25$) alloys were synthesized, and their microstructure and hydrogen storage properties were analyzed. The alloys featured both a primary Mg₂Ni phase and a

Mg–Mg₂Ni lamellar structure. With increasing Ni content, there was a notable decrease in the maximum hydrogen storage capacity, attributable to the rising proportion of the Mg₂Ni phase. Despite the variations of Ni content, the first and second plateau pressures remained consistent across all three alloys. Thermodynamic calculations predicted that the compositions of the Mg and Mg₂Ni phases would remain unchanged in the alloys, despite the differing Ni contents. The compositions of the Mg and Mg₂Ni phases in the alloys were analyzed by TEM. The Mg phase consisted of 100% Mg, and the composition of the Mg₂Ni phase closely matched theoretical stoichiometry. Hence, it was established that variations in Ni content did not influence the plateau pressure in the hyper-eutectic Mg–Ni alloys, as the compositions of the Mg and Mg₂Ni phases remained consistent.

Declaration of competing interest

The authors declare that they have no known competing financial interests or personal relationships that could have appeared to influence the work reported in this paper.

Acknowledgments

This research was supported by the National Research Foundation of Korea (NRF) funded by the Ministry of Science and ICT (Grant No. 2022M3D1A2095316), the Korea Institute of Industrial Technology (KITECH EH-24-0007), and the National Research Council of Science & Technology (NST) grant by the Korea government (MSIT) (No. GTL24051-300).

References

- [1] Lcellent C, Gondor G. Analysis of hydride formation for hydrogen storage: pressure–composition isotherm curves modeling. *Intermetallics* 2007;15(7): 934–44. <https://doi.org/10.1016/j.intermet.2006.11.002>.
- [2] Lee DH, Im HT, Kwon HG, et al. A study on the first hydrogenation behavior of TiFe_{0.9}Cr_{0.1} hydrogen storage alloy with the laves phase. *Int J Hydrogen Energy* 2024;56:864–70. <https://doi.org/10.1016/j.ijhydene.2023.12.180>.
- [3] Kwon HG, et al. Microstructural study on the slope of plateau pressure in TiFe_{0.9}Al_{0.1} hydrogen storage alloy. *Mater Lett* 2024;360:135951. <https://doi.org/10.1016/j.matlet.2024.135951>.
- [4] Kwon HG, et al. Study on the microstructure and hydrogen storage property changes of cast TiFe_{0.9}Cr_{0.1} alloy by homogenization annealing. *Mater Chem Phys* 2023;309:128362. <https://doi.org/10.1016/j.matchemphys.2023.128362>.
- [5] Park KB, et al. On the first hydrogenation kinetics and mechanisms of a TiFe_{0.95}Cr_{0.05} alloy produced by gas atomization. *Mater Charact* 2022;192:112188. <https://doi.org/10.1016/j.matchar.2022.112188>.
- [6] Züttel A. Materials for hydrogen storage. *Mater Today* 2003;6(9):24–33. [https://doi.org/10.1016/S1369-7021\(03\)00922-2](https://doi.org/10.1016/S1369-7021(03)00922-2).
- [7] Luo Q, et al. Kinetics in Mg-based hydrogen storage materials: enhancement and mechanism. *J Magnes Alloys* 2019;7(1):58–71. <https://doi.org/10.1016/j.jma.2018.12.001>.
- [8] Shao H, et al. Progress and trends in magnesium-based materials for energy-storage research: a review. *Energy Technol* 2018;6(3):445–58. <https://doi.org/10.1002/ente.201700401>.
- [9] Huot J, et al. Mechanochemistry of metal hydrides: recent advances. *Mater* 2019; 12(17):2778. <https://doi.org/10.3390/ma12172778>.
- [10] Botta WJ, et al. Metallurgical processing of Mg alloys and MgH₂ for hydrogen storage. *J Alloys Compd* 2022;897:162798. <https://doi.org/10.1016/j.jallcom.2021.162798>.
- [11] Wen J, Rango P, et al. Improving hydrogen storage performance of Mg-based alloy through microstructure optimization. *J Power Sources* 2020;480:228823. <https://doi.org/10.1016/j.jpowsour.2020.228823>.
- [12] Panda S, Fundenberger JJ, et al. Effect of initial powder type on the hydrogen storage properties of high-pressure torsion consolidated Mg. *Int J Hydrogen Energy* 2017;42(35):22438–48. <https://doi.org/10.1016/j.ijhydene.2017.05.097>.
- [13] Imamura H, Masanari K, et al. High hydrogen storage capacity of nanosized magnesium synthesized by high energy ball-milling. *J Alloys Compd* 2005;386 (1–2):211–6. <https://doi.org/10.1016/j.jallcom.2004.04.145>.
- [14] Ouyang L, Liu F, et al. Magnesium-based hydrogen storage compounds: a review. *J Alloys Compd* 2020;832:154865. <https://doi.org/10.1016/j.jallcom.2020.154865>.
- [15] Bogdanović B, Reiser A, et al. Thermodynamics and dynamics of the Mg–Fe–H system and its potential for thermochemical thermal energy storage. *J Alloys Compd* 2002;345(1–2):77–89. [https://doi.org/10.1016/S0925-8388\(02\)00308-0](https://doi.org/10.1016/S0925-8388(02)00308-0).
- [16] Li Q, Lu Y, et al. Thermodynamics and kinetics of hydriding and dehydriding reactions in Mg-based hydrogen storage materials. *J Magnes Alloy* 2021;9(6): 1922–41. <https://doi.org/10.1016/j.jma.2021.10.002>.

- [17] Puszkiel J, Gennari F, et al. Sorption behavior of the MgH₂-Mg₂FeH₆ hydride storage system synthesized by mechanical milling followed by sintering. *Int J Hydrogen Energy* 2013;38(34):14618–30.
- [18] Khan D, Panda S, et al. Formation and hydrogen storage behavior of nanostructured Mg₂FeH₆ in a compressed 2MgH₂–Fe composite. *Int J Hydrogen Energy* 2020;45(41):21676–86. <https://doi.org/10.1016/j.ijhydene.2020.06.025>.
- [19] Orimo S, Fujii H. Materials science of Mg-Ni-based new hydrides. *Appl Phys A* 2001;72:167–86. <https://doi.org/10.1007/s003390100771>.
- [20] Cermak J, Kral L. Hydrogen diffusion in Mg–H and Mg–Ni–H alloys. *Acta Mater* 2008;56(12):2677–86. <https://doi.org/10.1016/j.actamat.2008.02.003>.
- [21] Li L, Akiyama T, et al. Hydriding and dehydriding behavior of the product in hydriding combustion synthesis of Mg₂NiH₄. *J Alloys Compd* 1999;287(1–2):98–103. [https://doi.org/10.1016/S0925-8388\(99\)00045-6](https://doi.org/10.1016/S0925-8388(99)00045-6).
- [22] Chen R, Ding X, et al. Tunable eutectic structure and de-/hydrogenation behavior via Cu substitution in Mg–Ni alloy. *J Power Sources* 2018;401:186–94. <https://doi.org/10.1016/j.jpowsour.2018.08.086>.
- [23] Nogita K, Ockerl S, et al. Engineering the Mg–Mg₂Ni eutectic transformation to produce improved hydrogen storage alloys. *Int J Hydrogen Energy* 2009;34(18):7686–91. <https://doi.org/10.1016/j.ijhydene.2009.07.036>.
- [24] Cao W, Ding X, et al. Enhanced de-/hydrogenation kinetics of a hyper-eutectic Mg₈₅Ni_{15-x}Ag_x alloy facilitated by Ag dissolving in Mg₂Ni. *J Alloys Compd* 2022;917:165457. <https://doi.org/10.1016/j.jallcom.2022.165457>.
- [25] Fadonougbo JO, Kim HJ, et al. Kinetics and thermodynamics of near eutectic Mg–Mg₂Ni composites produced by casting process. *Int J Hydrogen Energy* 2020;45(53):29009–22. <https://doi.org/10.1016/j.ijhydene.2021.11.025>.
- [26] Fadonougbo JO, Kim HJ, et al. On the long-term cyclic stability of near-eutectic Mg–Mg₂Ni alloys. *Int J Hydrogen Energy* 2022;47(6):3939–47. <https://doi.org/10.1016/j.ijhydene.2021.11.025>.
- [27] Ding X, Chen R, et al. Activation mechanism and dehydrogenation behavior in bulk hypo/hyper-eutectic Mg–Ni alloy. *J Power Sources* 2018;374:158–65. <https://doi.org/10.1016/j.jpowsour.2017.11.034>.
- [28] Shang Y, Pistidda C, et al. Mg-based materials for hydrogen storage. *J Magnes Alloy* 2021;9(6):1837–60. <https://doi.org/10.1016/j.jma.2021.06.007>.
- [29] Ko WS, Park KB, et al. Density functional theory study on the role of ternary alloying elements in TiFe-based hydrogen storage alloys. *J Mater Sci Technol* 2021;92:148–58. <https://doi.org/10.1016/j.jmst.2021.03.042>.
- [30] Park KB, Fadonougbo JO, et al. Effect of Fe substitution on first hydrogenation kinetics of TiFe-based hydrogen storage alloys after air exposure. *Int J Hydrogen Energy* 2021;46(60):30780–9.
- [31] Fadonougbo JO, Park KB, et al. An integrated computational and experimental method for predicting hydrogen plateau pressures of TiFe_{1-x}Mx-based room temperature hydrides. *Int J Hydrogen Energy* 2022;47(40):17673–82. <https://doi.org/10.1016/j.ijhydene.2022.03.240>.
- [32] Slater JC. Atomic radii in crystals. *J Chem Phys* 1964;41(10):3199–204. <https://doi.org/10.1063/1.1725697>.